A Wireless Robot for Networked Laparoscopy

Cristian A. Castro, Adham Alqassis, Sara Smith, Thomas Ketterl, Yu Sun, Sharona Ross,
Alexander Rosemurgy, Peter P. Savage, and Richard D. Gitlin*

Abstract—State-of-the-art laparoscopes for minimally invasive abdominal surgery are encumbered by cabling for power, video, and light sources. Although these laparoscopes provide good image quality, they interfere with surgical instruments, occupy a trocar port, require an assistant in the operating room to control the scope, have a very limited field of view, and are expensive. *MARVEL* is a wireless Miniature Anchored Robotic Videoscope for Expedited Laparoscopy that addresses these limitations by providing an inexpensive *in vivo* wireless camera module (CM) that eliminates the surgical-tool bottleneck experienced by surgeons in current laparoscopic endoscopic single-site (LESS) procedures. The MARVEL system includes 1) multiple CMs that feature a wirelessly controlled pan/tilt camera platform, which enable a full hemisphere field of view inside the abdominal cavity, wirelessly adjustable focus, and a multiwavelength illumination control system; 2) a master control module that provides a near-zero latency video wireless communications link, independent wireless control for multiple MARVEL CMs, digital zoom; and 3) a wireless human–machine interface that gives the surgeon full control over CM functionality. The research reported in this paper is the first step in developing a suite of semi-autonomous wirelessly controlled and networked robotic cyber-physical devices to enable a paradigm shift in minimally invasive surgery and other domains such as wireless body area networks.

Index Terms—*In vivo* wireless networking, minimally invasive surgery (MIS), robotic videoscope.

I. INTRODUCTION

MINIMALLY invasive surgery (MIS) and particularly laparoscopic endoscopic single-site (LESS) procedures

C. A. Castro, A. Alqassis, and T. Ketterl are with the Electrical Engineering Department, University of South Florida, Tampa, FL 33620 USA (e-mail: cacastr3@mail.usf.edu; aalqassi@mail.usf.edu; ketterl@usf.edu).

S. Smith is with the Industrial Engineering Department, University of South Florida, Tampa, FL 33620 USA (e-mail: stsmith7@mail.usf.edu).

Y. Sun is with the Computer Science Engineering Department, University of South Florida, Tampa, FL 33620 USA (e-mail: yusun@cse.usf.edu).

S. Ross was with the College of Medicine, University Of South Florida, Tampa, FL 33620 USA. He is now with the Southeastern Center for Digestive Disorders and Pancreatic Cancer, Advanced Minimally Invasive and Robotic Surgery, Florida Hospital, Tampa, FL 33613 USA (e-mail: sross@health.usf.edu).

A. Rosemurgy was with Center for Digestive Disorders, Tampa General Hospital, Tampa, FL 33606 USA. He is now with the Southeastern Center for Digestive Disorders and Pancreatic Cancer, Advanced Minimally Invasive and Robotic Surgery at Florida Hospital, Tampa, FL 33613 USA (e-mail: arosemur@health.usf.edu).

P. P. Savage is with Innovatia Medical Systems LLC, Tampa, FL 33701 USA (e-mail: pete@innovatiamedical.com).

*R. D. Gitlin is with the Electrical Engineering Department, University of South Florida, Tampa, FL 33620 USA (e-mail: richgitlin@usf.edu).

Color versions of one or more of the figures in this paper are available online at http://ieeexplore.ieee.org.

Digital Object Identifier 10.1109/TBME.2012.2232926

reduce damage to biological tissues and decrease rehabilitation time [1]. While these procedures have revolutionized MIS, laparoscopes available for MIS and LESS procedures are inconvenient for the following reasons. First, they require access to the abdominal cavity either through a separate incision or through a port in a multiport access trocar. Second, they have a limited field of view inside the abdominal cavity. Third, the laparoscope interferes with surgical instruments, and the videoscope cables for light, video imaging, and power clutter the operating room. Finally, conventional laparoscopes require an assistant to control the scope and to produce stable views of the operating site.

Many studies have addressed these limitations. Researchers at Vanderbilt University designed and tested a wired single-port camera that uses an external magnetic field and a robotic internal active magnetic levitation system to produce a precise tilt motion [2]. Researchers at the University of California at Los Angeles [3] produced a device that provides views of the surgical site and surrounding anatomy from multiple angles using a surgical "polyvisiometric" camera. A device developed by University of Colorado researchers features a single-port camera and an integrated display system that modifies a grasper tool to hold an external display and the internal vision system [4]. Research on endoscopic cameras by Columbia University [5], [6] includes two distinct prototypes, one with a single camera and another with a stereoscopic camera, allowing for the possibility of depth perception, but with an increased diameter. The Columbia cameras feature low-power, high-efficiency pan/tilt mechanisms and have pinhole lenses. At the University of Nebraska, Lincoln [7], [8], work has been done on a robotic camera system that moves through the abdominal cavity while tethered to a supporting cable for power and video interfacing. Recent work at The BioRobotics Institute, Scuola Superiore Sant'Anna, Pisa, Italy [9], resulted in the design of three 12-mm-diameter modular robotic units: a camera, a retractor and a manipulator unit, and the assembly and testing of the camera unit.

While each of these studies address some of the limitations highlighted previously, none of them resolves all the drawbacks of the laparoscopes available for MIS and LESS procedures. The research described in this paper solves these problems, and it takes the next step in advancing the MIS paradigm with the design of a wireless *M*iniature and *A*nchored *R*obotic *V*ideoscope for *E*xpedited *L*aparoscopy (MARVEL) platform, a cable-free platform placed within the operating cavity prior to surgical procedures. This platform removes the need for additional incisions in the abdomen, provides better visualization of the operating cavity, and frees a port in single-site multiport trocars allowing greater dexterity for surgeons and insertion of additional surgical tools for safer and more efficient procedures.
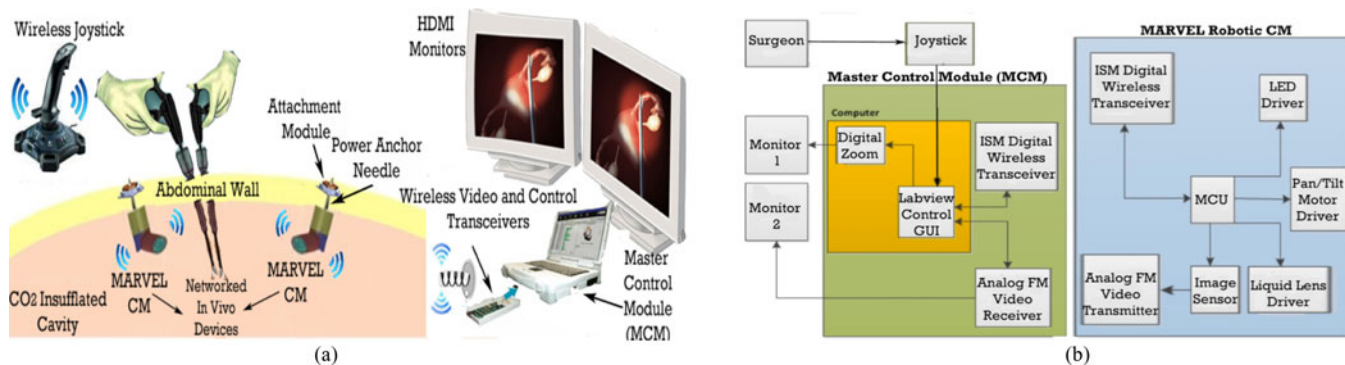
Fig. 1. (a) Functional diagram of the MARVEL system, including the MCM and the MARVEL robotic CM. (b) MARVEL system physical configuration, showing two networked CMs, a wireless joystick interface and the MCM.
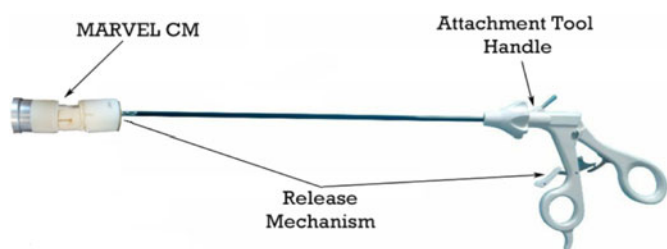

Fig. 2. Customized insertion removal tool used for attaching the MARVEL platform within the peritoneal cavity. MARVEL provides its own imaging during attachment eliminating the need for a cabled laparoscope at any portion of the procedure.

The outline of this paper is as follows. Section II provides an overview of the system described in previous work [10]. Section III describes the *in vivo* wireless channel simulation model used to characterize wireless video communication through the human body. Section IV describes simulation, characterization, and experimental validation of the illumination subsystem. Section V explains wirelessly adjustable focus and digital zoom added to improve visualization and imaging, as well as system validation and characterization of the imaging subsystem. Section VI discusses the *in vivo* experiment conducted to validate the entire system and the *in vivo* wireless channel model. Section VII presents conclusions and suggestions for future research.

II. MARVEL CONCEPT

A. System Overview

The MARVEL system is comprised of a master control module (MCM), a wireless human–machine interface (HMI), and the MARVEL camera modules (CMs) (see Fig. 1). When this device is used in LESS procedures, the surgeon first inserts each CM into the end of a custom-designed insertion/removal tool (see Fig. 2) A coaxial needle, which is part of the camera platform, is used to secure and power the CM during insertion and removal, while the CM is attached to the abdominal wall. The CM is secured to the abdominal wall without using a separate videoscope for assistance.

The surgeon controls the CM by a wireless joystick as the HMI. The joystick controls pan/tilt movement, adjustable focus, illumination, and digital zoom of all of the *in vivo* CMs. The MCM processes signals coming from the joystick.

The MCM controls the entire system. It is here that wireless video coming from each CM is processed, digital zoom is implemented, and wireless control datagrams are generated. Once the MCM processes the joystick commands, a datagram is passed to the wireless digital ISM-band wireless transceiver and broadcast to the MARVEL CMs as shown in Fig. 1. The datagram is processed by the embedded microcontroller in the CMs and then transformed into corresponding control signals for the pan/tilt motors, a liquid crystal lens (LCL) driver, an image sensor, and an LED driver. Each CM wirelessly sends its video stream to the MCM, which displays the images on high-resolution monitors. Once video is transmitted from the CMs to the MCM, a C++ application receives the digital zoom in/out commands from the joystick and postprocesses the transmitted video by effectively cropping and expanding the pixel area of the original image.

The MARVEL CM robotic platform is composed of five subsystems: 1) the illumination subsystem, which provides light inside the abdominal cavity; 2) the imaging subsystem, which provides optimal focus and video resolution; 3) the wireless communication subsystem, which implements control commands and video communication between the device and the MCM; 4) the embedded control subsystem, which handles the control decision making for the device; and 5) the attachment needle power subsystem, which secures the CM to the abdominal wall and powers the CM (future CMs will be battery powered).

The MCU of the CM uses a serial peripheral interface (SPI) to acquire the wireless data coming from the ISM digital transceiver IC (CC1101) and an I2C interface to control the LCL driver in 40 steps. The motor control commands are implemented by four pulse-width modulation (PWM) signals at 24 kHz interfaced with an H-bridge dual motor driver. The speed of the pan motor can be changed from 0.48 to 31 r/min and the speed of the tilt motor can be changed from 0.24 to 17 r/min, giving the surgeon smooth control. Three general-purpose input/output (GPIO) lines control the step-up converter for LED
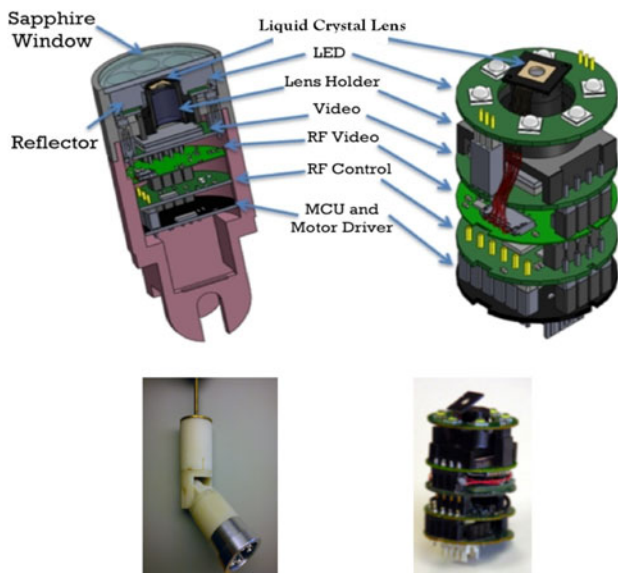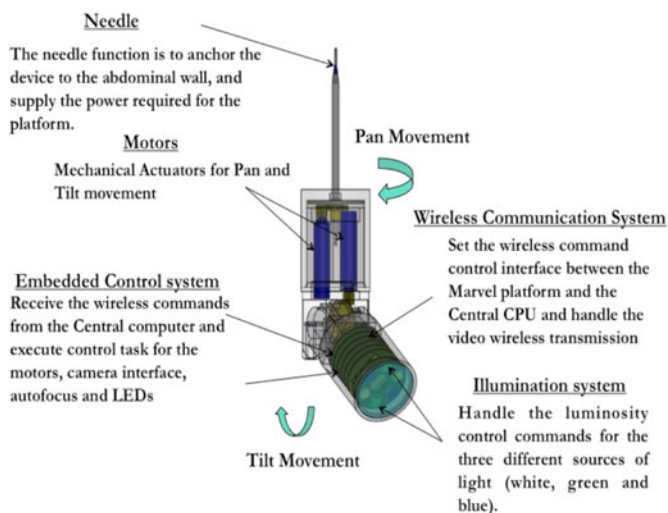
Fig. 3.   Top: MARVEL CAD model. Middle: MARVEL system interconnection, a total of 18 internal signals are going through the whole stack of PCBs. Bottom: MARVEL research platform.

Fig. 4.   Top: MARVEL vision system exploded view. Bottom left: LCL. Bottom right: Assembled LED system.

intensity control. Each of the lines carries a PWM signal at 400 Hz, which can be set to 256 different levels.

Each MARVEL CM contains five PCBs in a modular design (see Fig. 3). Each PCB has two connectors that allow for easy integration of new and/or additional designs into the system. The interconnection system provides two digital control buses: an inter-IC (I2C) bus and an SPI bus throughout the PCB stack.

Fogging in the MARVEL CM was prevented by an antifog lens cleaner applied to both sides of the glass window. The MARVEL CMs were sealed to guarantee no leakage.

B. Wireless Adjustable Focus

Fig. 4 shows the CAD model of the video imaging subsystem, which consists of 1) a customized Sunex lens holder; 2) a 1/2.7″ Sunex lens with a focal length of 4.37 and a focal range between 60 and 100 mm at a maximum of 2M pixels; 3) a LensVector LCL which changes focus by varying voltage applied across the

lens changing from 0 to +10 diopters; and 4) an OmniVision OV7949 video image sensor with a sensitivity of 4.6 V/Lux-sec, an imaging array of 510×496 pixels, and a pixel size of $9.2~\mu\text{m} \times 7.2~\mu\text{m}$. The combination of the LensVector LCL and the fixed lens extended the focal range of the CM by 20 cm. The LCL replaces the complex, bulky, and often-fragile traditional mechanical focus approach of current CMs.

III. *In Vivo* WIRELESS CHANNEL MODEL

The *in vivo* wireless channel is very different from the classic multipath wireless communication medium used for cellular or wireless LAN service. Since the electromagnetic wave passes through multiple media with different electrical properties, the wave propagation speed is significantly reduced and may induce significant time dispersion (propagation delay that varies with frequency) that is different for each organ and body tissue.

An understanding of how RF signals propagate inside, through and near the human body, is necessary to optimize transmitter, receiver, antenna designs, communication algorithms, and protocols. One method that can be used to calculate *in vivo* channel characteristics without using live test subjects uses high-frequency electromagnetic simulation software. Simulators that use finite-element methods (FEM) to solve for RF field interactions are approved by the FCC for use in the design of implantable wireless devices [11].

We used the ANSYS HFSS [12] high-frequency electromagnetic field simulator to derive the *in vivo* channel model. This software calculates the total RF field in 3-D space generated from arbitrarily designed and placed antennas in the simulated environment over a wide frequency range. ANSYS also provides a physically and electrically accurate human body model that can be used to model the RF field interactions with human body tissues in HFSS. The model includes over 300 muscles, organs, bones, and other tissues with a dimensional accuracy of 1 mm. Frequency-dependent conductivity and permittivity for
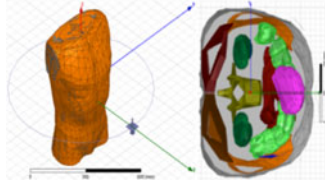
Fig. 5. Right: CAD drawing of the HFSS human body model used to derive the *in vivo* channel model. Left: Side view of a torso and a cross-sectional top view.
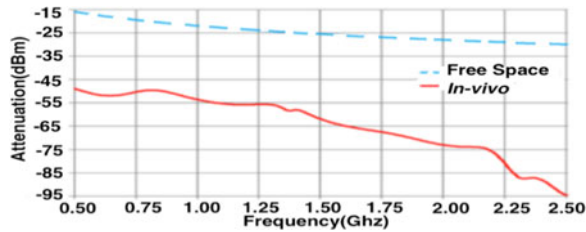

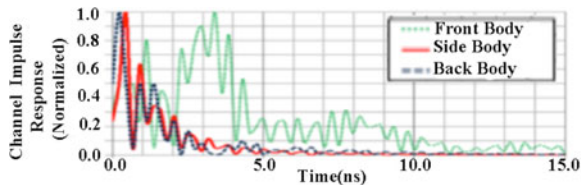Fig. 6. *In vivo* and free space wireless attenuation as a function of frequency.

Fig. 7. CIR of signals traveling in different directions through the human body.

each organ and tissue are included in the model, accurate from 20 Hz to 20 GHz.

Fig. 5 shows an example where the head, legs, and arms were removed to reduce computation time, since the removed body parts would have very little effect on RF propagation. The figure also shows the location of the external receive antenna at the same height as the transmit antenna.

The simulated attenuation of the transmitted signal from the model used in Fig. 5 is shown in Fig. 6. The plot of the attenuation of a signal through free space is also shown for comparison. A significant increase in attenuation is seen, and the attenuation rate is not constant with frequency, similar to free-space transmission losses.

Another example where the use of simulated channel characteristics is useful is in calculation of the impulse channel response (CIR) derived from attenuation data found in the *in vivo* simulations. A CIR provides a mathematical description of how a transmitted signal is affected in the time domain as it travels through the channel. The CIR contains information to characterize how a linear communication system will perform when operating in a given channel. We compared the calculated CIRs of signals traveling through the side, front, and back of the body and found through these channel impulse calculations (see Fig. 7) that the dispersion is greatest when the signal passes from the inside through the abdomen of the body. The higher dispersion is most likely because the RF signal encounters more organs (stomach, intestines, bladder, etc.) as it traverses through
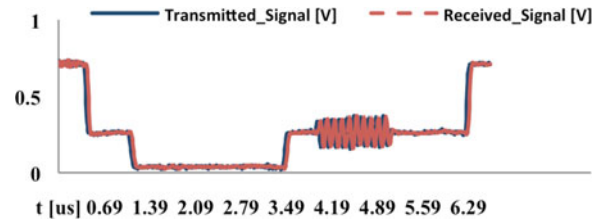

Fig. 8. Comparing the transmitted composite signal to the received signal through the human body simulation.

the abdomen, which present a greater amount of frequency-dependent variations to the signal.

These results show signal attenuation through the human body and the derived CIR is vastly different from classical wireless cellular propagation models and indicates the need for accurate characterization for the MARVEL system [13]. We used the RF *in vivo* channel characteristics obtained from these simulations to verify the wireless video signal generated by the MARVEL wireless transmitter system, as described in [10], which is not compromised beyond an acceptable level; i.e., signal attenuation, distortions, and latency affects are kept to a minimum to ensure that a high-quality video image can be received. This was done by sampling a portion of the composite image, generated by the image sensor, and passing it through the *in vivo* CIR derived from HFSS in software simulation. The transmitted signal, after passing through the simulated channel, can then be compared to the original signal. A comparison between the transmitted and received signals is shown in Fig. 8. Insignificant signal integrity issues were observed in this simulation with the transmitter system, the modulation scheme, and the frequency of operation chosen for the MARVEL CM.

IV. SYSTEM VALIDATION AND *In Vivo* EXPERIMENT

A complete characterization and validation for each one of the MARVEL subsystems was first done by simulations and later tested through a series of bench experiments.

A. Illumination Subsystem

The illumination subsystem plays a significant role in achieving the desired performance of laparo-endoscope devices. Color definition and image quality are intimately related to the source of light inside the abdominal cavity. TracePro software [14] was used to characterize the LED intensity distribution and the reflector cone shape. It is a comprehensive, versatile software tool for modeling the propagation of light in imaging and nonimaging optomechanical systems.

Fig. 9 shows the geometry of the LED light distribution model used in the simulation. The upper disk is the geometrical area through which the simulation program calculates the ray traces. For consistency, the LED emission flux was about 1 W, the angular distribution was Lambertian, with a wavelength of 500 nm, and about 4000 rays were emitted in total. The cone reflector had a 100% reflectivity on the cavity surface. A disk calculation target area (the upper large disk in Fig. 9) had a radius of 20 mm and was set 20 mm away from the LED base. That distance
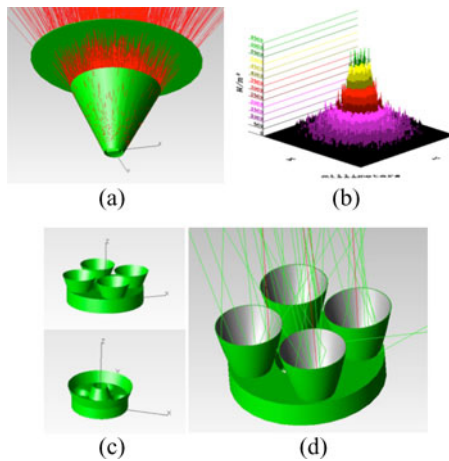
Fig. 9. (a) Geometry of the LED light distribution experimental model in TracePro, showing the LED and cone reflector. The upper large disk is the geometrical area through which the TracePro program calculates the ray tracing. (b) LED light pattern simulation ($f = 0.4$ mm parabolic reflector; relative Intensity), measured at distances of 5 cm from the LED sources. (c) CAD drawing of two reflector geometries used by the simulation. (d) LED ring with individual reflectors showing predicted optical ray tracing.

corresponds to a $\pm 45°$ viewing angle. The cone reflectors had the same parameters as those used in the actual implementation and included cones with half angles of $10°$, $20°$, and $30°$. As can be seen in Fig. 9, most of the rays hit the calculation target area.

A test bench experiment was designed to confirm the simulation results. A Si photodiode (PIN SC/10D, UDT Sensors Inc.) measured light intensity at different distances from the LED. The dimension of the sensor area was 10 mm $\times$ 10 mm. Tests of the active area of the detector indicated equal sensitivity over the surface area. The maximum recommended incident power density is 10 mW/cm^2. Typical uniformity of response for a 1 mm spot size was $\pm 2\%$. The anode of the photodiode detector was connected to the negative electrode and the cathode of the photodetector was connected to the positive electrode of the oscilloscope. We expect the photocurrent to be linearly proportional to the luminance. The relative flux density of the ray tracings (or light intensity) was plotted as a function of the angle from the LED surface. Fig. 10 shows the LED light distribution predicted using the TracePro software and the experimental result. These results indicate that the $10°$ and $20°$ angle cone reflectors produced significant increases in the light hitting the target.

B. Video Imaging Subsystem

In order to evaluate the Sunex lens and the LensVector LCL, an optical test bench was built to compare the focus range of the lens systems. Fig. 11 shows an image of the resolution test chart at a distance of 15 mm and with the same focus, the chart at a distance of 110 mm. The focus and the sharpness were not affected when the chart was positioned at a further distance. The integration of the Sunex and LensVector lenses results in a 10 diopter change maximizing the quality and sharpness of the image.

To ensure reliability and functionality of the video imaging subsystem, a test was designed to measure the effective focus range and zoom capabilities of the CMs. The test consisted of
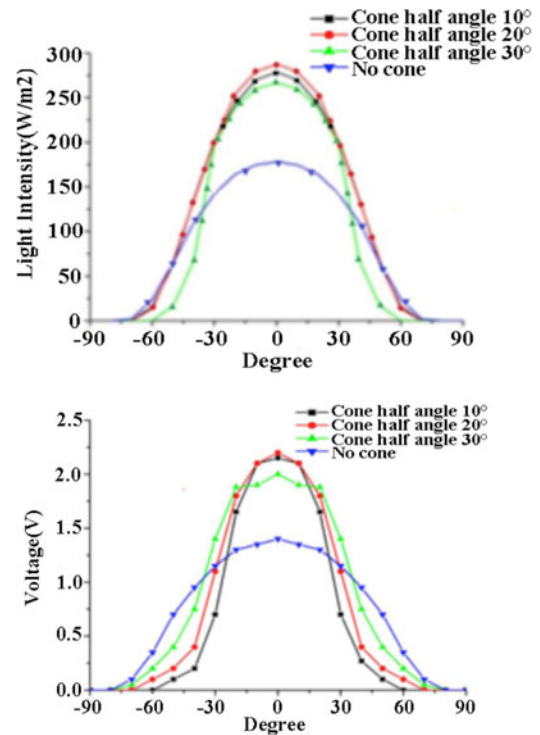

Fig. 10. Top: TracePro LED light distribution at 5 cm from the target. Bottom: Measured LED light distribution using different light reflecting cones; distance was 5 cm.
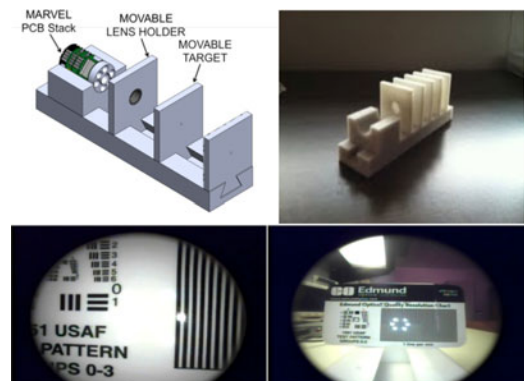

Fig. 11. Top: CAD design and final prototype of the test bench. Bottom: Captured images using Sunex lens and the lens vector liquid crystal at 15 and 110 mm.

Fig. 12. Focus and digital zoom test fixtures with a phantom human organ model.

1) focus and sharpness at different target positions and 2) digital zoom ranges without significant loss in resolution. Two CMs were placed inside a clear plastic box as seen in Fig. 12.

An image of human organs was placed inside a phantom model to provide a view of what would be seen in a surgical procedure. The phantom model was placed at distances of 50–150 mm, which is the range required during surgery. Fig. 13

Fig. 13. Top left: Original image. Top right: Zoomed image. Bottom left: Unfocused image. Bottom right: Focused image.
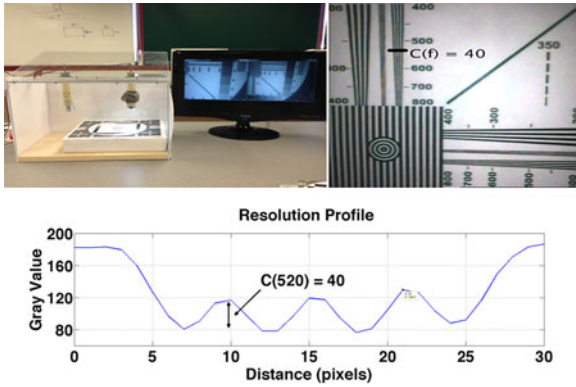

Fig. 14. Top: Test fixture and resolution chart used to measure the MARVEL CM resolution. Bottom: Resolution profile showing the contrast ratio equal to 40. This happens approximately at 520 horizontal lines in the resolution chart (horizontal black mark).

shows the phantom model placed at 76 mm from the CM. We can observe the difference in image sharpness as the focus was adjusted wirelessly from the joystick. Digital zoom testing was also accomplished using the phantom model in Fig. 13. When the resolution of the selected area for zooming is less than half of the display resolution, the zoomed-in video loses sharpness [15].

The resolution of the CMs was characterized using the setup shown in Fig. 14. A CM was positioned above a resolution chart so the chart filled the field of view of the CM; the zoom was set to zero, the focus set to maximize the sharpness of the camera, and the LED light set to 550 lm at 5000 K color temperature. The modulation transfer function (MTF) defined in (1), where $C(0)$ is the low-frequency (black–white) contrast ratio and $C(f)$ is the contrast ratio at spatial frequency f, was used to measure system resolution. An MTF equal to 50% is the cut-off frequency for the resolution [16]. The MARVEL CM presents $C(0)$ equal to 80, for which $C(f)$ must be greater than or equal to 40, in order to guarantee a good image quality as shown in Fig. 14

$$\mathrm{MTF}(f) = 100\% * \frac{C(f)}{C(0)}. \tag{1}$$

C. In Vivo Experimental Evaluation

An *in vivo* experiment was conducted at the USF Vivarium. The IACUC protocol for the porcine animal study was approved
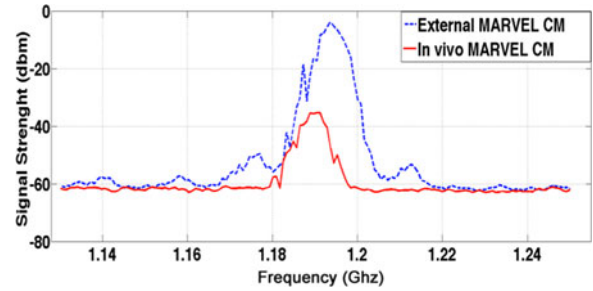

Fig. 15. MARVEL CM *in vivo* and external measured signal strength comparison.

prior to the surgical procedure. The surgeons used a trocar to penetrate the abdominal wall and an incision was made to insert the CMs 20 cm apart on either side of the major incision. The surgeon secured the CMs in place with an attachment module on the coaxial needle.

We compared the loss in signal strength of the transmitted video signal in two cases: one with the CM *in vivo* inside of the abdominal cavity and the second case with the same CM external to the porcine subject. The CM was kept at the same distance from the receive antenna (∼0.5 m) during both measurements. We used a spectrum analyzer to measure the signal strength of the modulated video signal over a 1.1–1.25 GHz band. Fig. 15 shows a comparison between captured signals. There is about a 30-dB difference in signal strength between the *in vivo* and external measurement caused by attenuation through body tissues. This is in agreement with a difference of 32 db as shown in Fig. 6. A slight "detuning" of the transmitted *in vivo* video signal can also be observed in Fig. 15. The center frequency of the modulated signal shifted from 1.193 to 1.190 GHz when placed inside the porcine body, most likely because of temperature differences between the inside and outside of the test animal. Most electronic components have variations in their electronic properties and values as a function of temperature, which can alter the modulation carrier frequency in the transmitter [17]–[19]. This shift in frequency did not create distortion in the transmitted video signal. Since the external receiver, described in [10], can receive a video signal between 1000 and 1200 MHz, a shifting of only 3 MHz does not impact the transmitted video signal. The receivers can be retuned manually to ensure that the video signal is not lost. In future devices, electronic components with lower temperature coefficients will be used to reduce the observed frequency shift. We will also shift to phase-locked-loop (PLL) receivers which can lock-on and track the frequency of the transmitted signal, eliminating the need for manual retuning.

The illumination subsystem of each CM was set to 550 lm, approximately 70% of the maximum light intensity. Power consumption was 368 mA in standby and 480 mA when pan and tilt motors were activated. The illumination subsystem consumed 200 mA (54% of the system power in standby mode), analog wireless video consumed 90 mA (24%), the video sensor consumed 43 mA (12%), and the MCU and digital transceiver consumed 35 mA (10%).

The surgeons wirelessly adapted the focus for each of the CMs (see Fig. 16). The focus range was 40–100 mm, the typical
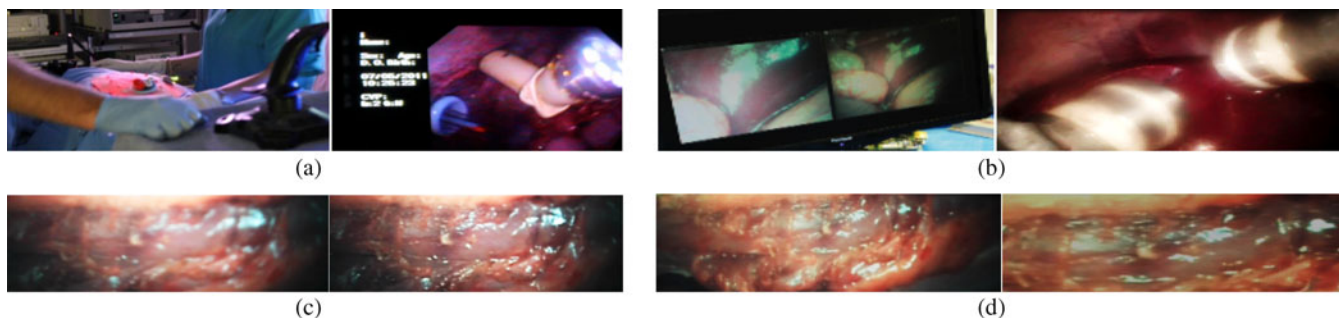
Fig. 16.   (a) MARVEL CM anchored to the abdominal wall. (b) Two MARVEL networked CMs are shown. The surgeons have independent control of each CM. High-definition monitor displaying normal and zoom images from the CMs. (c) Left: Unfocused and right focused images after using the wireless focus control capability of the CM. (d) Left: Normal video signal, right: image after a zoom in.

distance for minimally invasive abdominal surgery. Fig. 16 also shows the original and the zoomed image displayed on the monitor during the experiment. When the surgeon was working in the zoomed area, the surgeon was also able to monitor the surrounding areas to prevent unseen adverse affects. The zoom range was limited due to losses in image quality at higher zoom levels showing the importance of high-definition video for future CMs. A helix antenna was designed and positioned in a corner of the operating room in accordance with the ANSYS HFSS software simulation to increase the quality of the received signal. This antenna features circular polarization to reduce video loss due to MARVEL CM antenna pan and tilt movement. Each CM transmitted at different frequencies to provide simultaneous live imaging from each CM: one at 1.18 GHz and the other at 1.23 GHz.

V. CONCLUSION

The MARVEL system is intended to advance MIS in the field of robotic videoscopes, and to be the first step in developing semiautonomous wirelessly controlled and networked laparoscopic and other intelligent *in vivo* devices to enable a paradigm shift in MIS and related domains. Software simulation and system characterization of the wireless channel propagation in/out of the human body provided vital information that can be used to accelerate the design and prototyping of MARVEL devices and of next-generation self-contained wireless networked intrabody devices. Future work on the MARVEL research platform will include the implementation of wireless high-definition video, an improved illumination system which will include blue and green lights at wavelengths of 345–445 nm and 530–550 nm, and the implementation of novel asymmetrical wireless digital communications to improve quality, yet lessen the computation complexity of the embedded devices, which will allow the implementation of wireless body networks with much higher bandwidth.

REFERENCES

[1] J. R. Romanelli and D. B. Earle, "Single-port laparoscopic surgery: An overview," *Surg. Endoscopy*, vol. 23, no. 7, pp. 1419–1427, Jul. 2009.

[2] M. Simi, M. Silvestri, C. Cavallotti, M. Vatteroni, P. Valdastri, A. Menciassi, and P. Dario, "Magnetically activated stereoscopic vision system for laparoendoscopic single site surgery," *IEEE/ASME Trans. Mechatronics*, vol. PP, no. 99, pp. 1–12, 2012.

[3] P. Berkelman, P. Cinquin, J. Troccaz, J. Ayoubi, C. Letoublon, and F. Bouchard, "A compact, compliant laparoscopic endoscope manipulator," in *Proc. IEEE Int. Conf. Robot. Autom.*, 2002, pp. 1870–1875.

[4] B. S. Terry, A. D. Ruppert, K. R. Steinhaus, J. A. Schoen, and M. E. Rentschler, "An integrated port camera and display system for laparoscopy," *IEEE Trans. Biomed. Eng.*, vol. 57, no. 5, pp. 1191–1197, May 2010.

[5] T. Hu, P. K. Allen, N. J. Hogle, and D. L. Fowler, "Insertable surgical imaging device with pan, tilt, zoom and lighting," in *Proc. Int. Conf. Robot. Autom.)*, May 19–23, 2008, pp. 2948–2953.

[6] T. Hu, P. K. Allen, T. Nadkarni, N. J. Hogle, and D. L. Fowler, "Insertable stereoscopic 3D surgical imaging device with pan and tilt," in *Proc. IEEE/RAS-EMBS Int. Conf. Biomed. Robot. Biomechatron.*, Scottsdale, AZ, 2008, pp. 311–316.

[7] S. R. Platt, "Vision and task assistance using modular wireless in vivo surgical robots," *IEEE Trans. Biomed. Eng.*, vol. 56, no. 6, pp. 1700–1710, Jun. 2009.

[8] J. Hawks, M. Rentschler, L. Redden, R. Infanger, J. Dumpert, S. Farritor, D. Oleynikov, and S. Platt, "Towards an in vivo wireless mobile robot for surgical assistance," *Stud. Health Technol. Inf.*, vol. 132, pp. 153–158, 2008.

[9] G. Tortora, A. Dimitracopoulos, P. Valdastri, A. Menciassi, and P. Dario, "Design of miniature modular in vivo robots for dedicated tasks in minimally invasive surgery," in *Proc. IEEE/ASME Int. Conf. Adv. Intell. Mechatron.*, Jul. 2011, pp. 327–332.

[10] C. A. Castro, S. Smith, A. Alqassis, T. Ketterl, Y. Sun, S. Ross, A. Rosemurgy, and R. D. Gitlin, "MARVEL: A wireless miniature anchored robotic videoscope for expedited laparoscopy," in *Proc. IEEE Int. Conf. Robot. Autom.*, May 2012, pp. 2926–2931.

[11] J. F. Mologni, L. A. Percebon, M. A. R. Alves, and E. Braga, "Comments on the FCC approval of finite element method for biomedical transmitters," in *Proc. Microwave Optoelectron. Conf.*, 2011, pp. 565–569.

[12] ANSYS, Inc., PA, (Nov. 22, 2011) "ANSYS HFSS," [Online]. Available: http://www.ansoft.com/products/hf/hfss/.

[13] T. P. Ketterl, G. E. Arrobo, A. Sahin, T. J. Tillman, H. Arslan, and R. D. Gitlin, "*In Vivo* wireless communication channels," in *Proc. IEEE 13th Annu. Wireless Microwave Technol. Conf.*, 2012, pp. 1–3.

[14] Lambda Research Corporation, MA (2010). "TRACEPRO," [Online]. Available: http://lambdares.com/software_products/tracepro/]

[15] M. Goss and K. Wu, "Study of supersampling methods for computer graphics hardware antialiasing," HP Labs, Palo Alto, CA, Tech. Rep. 121R1, Dec. 5, 2000.

[16] M. Bravo-Zanoguera, J. Rivera-Castillo, M. Vera-Perez, and M. Reyna Carranza, "Use of the modulation transfer function to measure quality of digital cameras," in *Proc. 16th Int. Conf. Electron. Commun. Comput.*, 2006, p. 52.

[17] J. Wang, "Radiation characteristics of ingestible wireless devices in human intestine following radio frequency exposure at 430, 800, 1200, and 2400 MHz," *IEEE Trans. Antennas Propag.*, vol. 57, no. 8, pp. 2418–2428, Aug. 2009.

[18] W. G. Scanlon, B. Burns, and N. E. Evans, "Radiowave propagation from a tissue-implanted source at 418 MHz and 916.5 MHz," *IEEE Trans. Biomed. Eng.*, vol. 47, no. 4, pp. 527–534, Apr. 2000.

[19] L. C. Chirwa, P. A. Hammond, S. Roy, and D. R. S. Cumming, "Electromagnetic radiation from ingested sources in the human intestine between 150 MHz and 1.2 GHz," *IEEE Trans. Biomed. Eng.*, vol. 50, no. 4, pp. 484–492, Apr. 2003.